Effect of Gas Flow Rate in PECVD of Amorphous Silicon Thin Films for Interface Passivation of Silicon Heterojunction Solar Cells

*Ashutosh Pandey, Shrestha Bhattacharya, Jagannath Panigrahi, Sourav Mandal, and Vamsi Krishna Komarala**

Precursor gas flow rate variation (30–80 sccm) in the plasma-enhanced chemical vapor deposition (PECVD) process of intrinsic a-Si:H layer deposition using SiH_4/H_2 (equal ratio) plasma is explored and its effect on the i-a-Si:H/c-Si interface passivation is investigated. A window of intermediate gas flow rates is determined for good quality surface passivation of n-type c-Si. Maximum effective minority carrier lifetime (τ_{eff}) above 1 ms, implied open-circuit voltage (iV_{oc}) ≈ 710 mV, and low interface defect density (D_{it}) $\approx 3.5 \times 10^9\ cm^{-2}\ eV^{-1}$ are obtained at an intermediate gas flow rate. The $SiH_4:H_2$ discharge emission characteristics, and the a-Si:H film characteristics such as hydrogen concentration, film density, optical band gap, and refractive index, are also investigated. To examine the effect of the flow rate variation on the performance of the final device, front-junction silicon heterojunction solar cells are fabricated on n-type Si wafers, and $\approx 17\%$ efficient cells are fabricated with an open-circuit voltage (V_{oc}) close to 690 mV at an optimized gas flow rate. This study provided information related to the transient plasma instability, SiH_4 depletion, secondary reactions in the plasma, and flux of radicals toward the substrate for the film growth with a good level of surface passivation.

1. Introduction

Amorphous/crystalline silicon heterojunction (SHJ) solar cells have been driving interest in the photovoltaic community because of their record open-circuit voltage (V_{oc}) (≈ 750 mV) and photo-conversion efficiency (25%).[1–4] The development of SHJ solar cells can be linked to a remarkably good electronic passivation of the c-Si surfaces obtained with only a few nanometers thick intrinsic amorphous silicon (i-a-Si:H) films.[1] The dopant diffusion of the c-Si wafer is also entirely avoided by forming the carrier-selective contacts to c-Si with equally thin doped a-Si:H overlayers. The fully passivated silicon surfaces are separated from the highly recombination active metal contacts.

Aside from a much better temperature coefficient of the cell and other factors, another significant advantage is the lean low-temperature ($<200\,°C$) process for the fabrication of the entire cell. The a-Si:H films are usually deposited by plasma-enhanced chemical vapor deposition (PECVD) technique with pure SiH_4 or diluted SiH_4/H_2 plasmas. The a-Si:H films' characteristics, such as the density and type of Si–H bonding and the density of weak and dangling bond (DB) defects, grown by PECVD are influenced by the deposition parameters such as substrate temperature,[5,6] power density, pressure, dilution ratio,[7] and post-deposition treatments.[8] Apart from the film process parameters, understanding the dissociation of the precursor gasses (SiH_4 and H_2) and the role of chemical reactions inside the growth zone is also very decisive.[9,10]

The properties of the passivating i-a-Si:H films must be carefully optimized with various experimental conditions for the SHJ cells due to 5–10 nm thickness, which plays a critical role in optimizing charge carrier recombination rate and transport. For example, 1) plasma/gas-phase reactions; and 2) surface reactions on the substrate are two crucial process steps in film growth. Under this, 1) silane depletion in the plasma has become one important indicator; with highly depleted silane plasma, the better c-Si surface passivation is achieved with the improved effective carrier lifetimes as a function of input power, silane flow rate (FR), and total pressure[11]; 2) optimum silane dilution with hydrogen was considered to avoid the epitaxy at the interface and to promote device-grade amorphous silicon for the better passivation[7,12,13]; 3) substrate temperature of 200–230 °C, which provides the thermal relaxation of a film based on the growth conditions (island or continuous type of growth)[6]; and 4) gas pressure,[7] based on the consumption rate of silane and availability of H content to saturate the DBs, better c-Si surface passivation observed, which is close to the transition region between amorphous and microcrystalline silicon phases. A recent review also highlights some advances in c-Si surface passivation for SHJ applications using i-a-Si:H films, from "transition-zone to underdense" and even emerging "stack" concept.[14]

A. Pandey, S. Bhattacharya, J. Panigrahi, S. Mandal, V. K. Komarala
Department of Energy Science and Engineering
Indian Institute of Technology Delhi
New Delhi 110 016, India
E-mail: vamsi@iitd.ac.in

Very little has been reported on the influence of gas FR in the conventional radio frequency (RF)-PECVD process of thin a-Si:H layers for c-Si surface passivation. Understanding the effect of precursor gas FR into the reactor chamber and its impact on passivation quality may also be necessary, as it plays an essential role in the gas residence time and the depletion. This study reports the effect of precursor gas FR variation on the c-Si surface passivation with the i-a-Si:H layers by keeping the SiH_4/H_2 dilution ratio fixed ($R = 1$). The films' optical bandgap, density, and hydrogen content are systematically analyzed with gas FR variation by fixing the substrate temperature, gas pressure, and applied power density for the c-Si surface passivation, and finally, SHJ cell performance was also investigated based on these films.

2. Results and Discussion

### 2.1. Effect of Gas FR on c-Si Surface Passivation

The c-Si surface passivation by the i-a-Si:H films are investigated by varying the gas FR (30–80 sccm) in the process chamber and keeping other process parameters fixed: substrate temperature, gas pressure, power density, and dilution ratio ($R = 1$). The deposition time is adjusted accordingly to maintain the same thickness of ≈10 nm i-a-Si:H films for surface passivation using ellipsometry measurements. **Figure 1**a shows the effect of gas FR variation on the effective minority carrier lifetimes (τ_{eff}) of the symmetrically passivated c-Si wafers. The gas FR between 40 and 70 sccm has led to better c-Si surface passivation with lifetimes of around 1 ms. In contrast, the FRs of <40 sccm and >70 sccm have deteriorated the passivation quality. To understand the variation in the passivation quality of the textured c-Si surface with the gas FR, the in-situ optical emission spectroscopy (OES) technique is adopted to monitor the excited states of molecules/atoms after the plasma generation from the SiH_4 and H_2 gases. The OES technique has been beneficial in optimizing process parameters of a SiH_4/H_2 glow discharge plasma for the growth of device-grade amorphous/microcrystalline silicon thin films,[15] and for effective a-Si:H/c-Si interface passivation.[7,16]

The optical emissions from the excited species such as SiH*, Si*, and the H_α line in a SiH_4/H_2 plasma provide information about the radicals and competitive reactions that contribute to the growth of a-Si:H.[17] For example, the ratio of the intensities of Si* (288 nm) and SiH* (414 nm) is a measure of the electron temperature in the plasma and, as a result, shows whether the SiH_3 or $SiH_{x<=2}$ radicals dominantly contribute to the growth of a-Si:H.[15] H_α similarly indicates atomic H, and the ratio of intensities of H_α and SiH* can be used to detect the phase transition from amorphous to the nanocrystalline regime.[7,16] Figure 1b shows the optical emission spectrum of the SiH_4/H_2 discharge recorded for the 30 sccm FR, after the plasma is stabilized. The H_α intensity is lower (lower by order of magnitude) than that of the SiH*, and the trend is the same for all the FRs. The integrated intensity of SiH* is shown in the inset of Figure 1b, which is estimated using a procedure described by Howling et al.[18] The SiH* peak intensity increased linearly with the FRs up to 70 sccm, then dropped. These observations are correlated with the c-Si surface passivation in the later part of the discussion.

As observed from Figure 1a, we obtain a good level of c-Si surface passivation in a window of the intermediate FR between 40 and 70 sccm, wherein the measured τ_{eff} lies in the same ballpark (≈1 ms). However, the estimated implied V_{oc} (iV_{oc}) drops from a maximum of 710 mV for FR of 60 sccm to 695 mV when FR is increased to 70 sccm. If closely examined, the lifetime data presented in **Figure 2** are different on the higher injection level side, which determines the iV_{oc}. To deduce the interface recombination parameters such as D_{it} and Q_{eff}, the measured $\tau_{eff}(\Delta n)$ data are modeled using the calculation based on the a-Si:H/c-Si DBs interface recombination model.[19,20] The analysis is an extended SRH-recombination formalism, and an algorithm was developed initially by Girisch et al., to compute recombination parameters of the SiO_2/c-Si interface.[21] Figure 2 shows the representative $\tau_{eff}(\Delta n)$ data (symbols) of two i-a-Si:H/c-Si/i-a-Si:H passivation samples representing two different FRs. The dashed lines are the estimated lifetimes due to intrinsic recombination ($\tau_{int,R}$) after Richter's parameterization,[22] short-dashed lines are the bulk SRH lifetimes ($\tau_{SRH,bulk}$) (which is estimated from $\tau_{p0,bulk} = 2.5$ ms measured by quinhydrone-solution-based passivation scheme), the dashed-dot lines are calculated surface
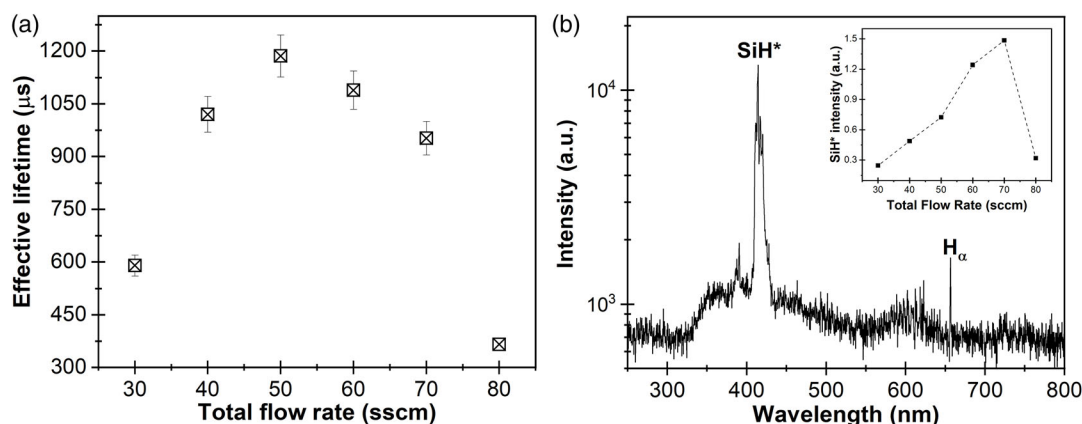
Figure 1. a) Effective minority carrier lifetimes (τ_{eff}) of the c-Si wafer passivated with ≈10 nm i-a-Si:H layers shown at an injection level of 10^{15} cm^{-3}, and b) a representative plot of the OE spectrum of SiH_4/H_2 discharge recorded for the flow rate (FR) of 30 sccm. Inset shows the integrated intensity of SiH* species at different gas FR.
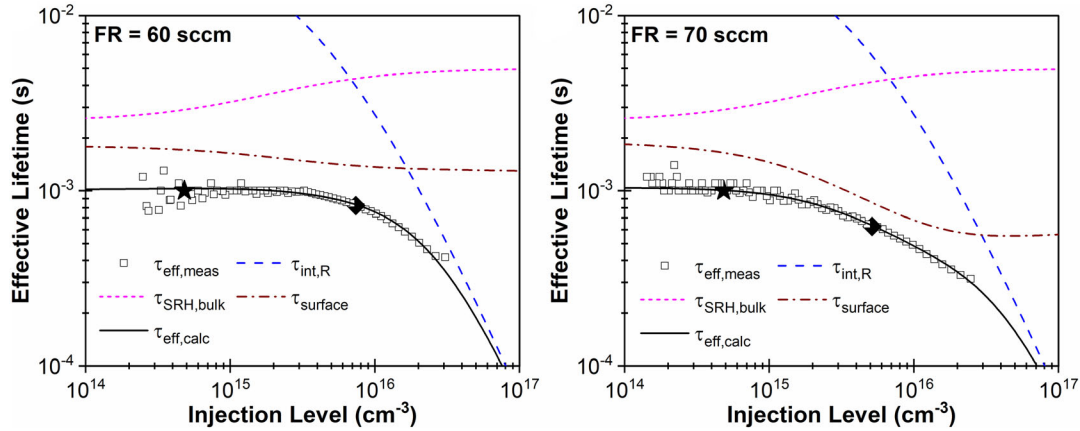
Figure 2. Representative plots of experimental effective minority carrier lifetime of c-Si wafers symmetrically passivated by ≈10 nm a-Si:H layers with gas FRs of 60 and 70 sccm. The lines are calculated lifetimes. The filled stars and diamonds indicate the $\tau_{eff}(\Delta n)$ values at maximum power point (MPP) and the open-circuit (OC) points, respectively.

lifetime ($\tau_{surface}$), and the continuous lines are calculated total effective lifetime ($\tau_{eff,calc}$), related by the formula

$$\frac{1}{\tau_{eff}} = \frac{1}{\tau_{int,R}} + \frac{1}{\tau_{SRH,bulk}} + \frac{1}{\tau_{surface}} \quad (1)$$

Only the parameters of the $\tau_{surface}$ are varied to model the experimental data. To calculate $\tau_{surface}$, for simplicity, an effective charge Q_{eff} that accounts for the charges in the amorphous layer as well as the interface charge is assumed and invoking the charge neutrality $Q_{Si} + Q_{eff} = 0$ condition, the band bending at the illuminated a-Si:H/c-Si interface is solved numerically using the MATLAB program. For the interface, DB states' capture cross-section ratios are set to be 1 and 10, respectively, for neutral (σ_n^0/σ_p^0) and charged (σ_n^+/σ_n^0 and σ_p^-/σ_p^0) states, as suggested by Leendertz et al.,[20] where $\sigma_p = 1 \times 10^{-16}$ cm^2, a typical value. The value of Q_{eff} is kept between 5 and 10×10^{10} cm^2. The error in deduced D_{it} and Q_{eff} is assumed to be 16% and 8%, respectively, arising from 8% uncertainty in the measurement of a lifetime in the transient mode. The measured $\tau_{eff}(\Delta n)$ data are converted into implied current density–voltage (J–V) curves,[23] from which the iV_{oc} at the 1 sun (iV_{oc}) and maximum power point voltage (iV_{mpp}) are obtained. The implied voltage is dependent on the value of Δn by the relation, $iV_{oc} = (kT/q)$ ln$[(\Delta n + N_D)\Delta n/n_i^2]$. For calculation of illumination-dependent current, J_{gen} of 38 mA cm^{-2} is used for the passivated structure, estimated using the Wafer Ray Tracer for the case of a Q-Flash w/IR filter spectrum. The implied voltages will be higher for high-quality passivation, and the OC and maximum power point (MPP) points will shift toward higher Δn values on a $\tau_{eff}(\Delta n)$ plot.

From Figure 2, the effect of the active dominant recombination in the high injection level side is apparent in the case of 70 sccm FR compared to 60 sccm FR. While the lifetime at the MPP is similar for both cases, the plots' surface lifetime shapes clearly affect the 1 sun lifetime; therefore, the iV_{oc}. After modeling the lifetime data, the lowest D_{it} ($<4.0 \times 10^9$ cm^{-2} eV^{-1}) is obtained for the intermediate FR of 60 sccm, which suggests the formation of a least defective

interface (as shown in **Figure 3**). In this case, the iV_{oc} and iV_{mpp} values are 710 and 609 mV, respectively. While for the FR of 70 sccm, the iV_{oc} is reduced to 695 mV because of an abrupt increase in $D_{it} \approx 9.0 \times 10^9$ cm^{-2} eV^{-1}, coupled with a slight asymmetry in the capture cross sections of the interfacial DB states ($\sigma_n^0/\sigma_p^0 = 2$–5). However, relatively high Q_{eff} in the layer maintains the MPP lifetime at 1 ms and, therefore, the iV_{mpp} remains above 600 mV. The values of the deduced interface D_{it} and calculated iV_{oc} are shown in Figure 3 for all six FR conditions. In the FR window of good quality passivation, higher iV_{oc} values (>700 mV) are obtained for the three FR conditions 40–60 sccm, while iV_{mpp} remains higher (>600 mV) for the whole FR window, including 70 sccm. The cause for this drop in iV_{oc} is due to dominant recombination through a high density of interface states at a higher injection level.
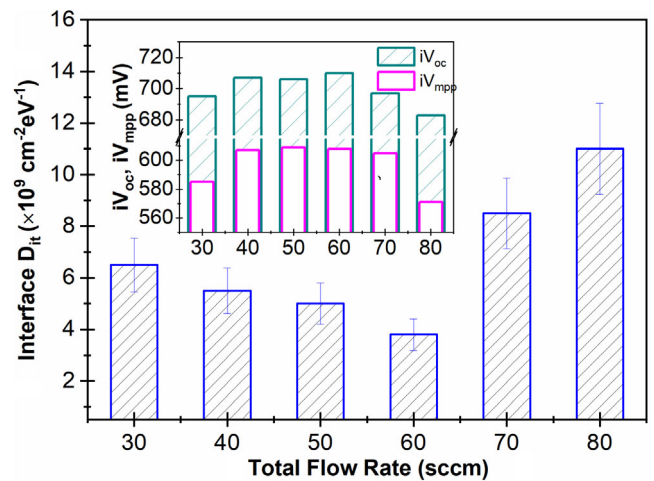
**Figure 3.** Variation of the interface defect states density (D_{it}) as a function of the total FR, deduced from modeling the measured $\tau_{eff}(\Delta n)$ data of the symmetrically passivated structures. Inset shows the iV_{oc} and iV_{mpp} extracted from the implied current density–voltage (J–V) curves converted from the measured $\tau_{eff}(\Delta n)$.

For high-quality passivation of the c-Si surface, the formation of transition-zone a-Si:H thin films with an abrupt interface are necessary,[24] and such films could be obtained under highly depleted SiH$_4$ plasma conditions.[11] Considering the only variable deposition parameter here is the FR, the plasma conditions that could be primarily affected are the SiH$_4$ depletion, plasma density, SiH$_2$/SiH$_3$ contribution ratio, the electron temperature, and the transient plasma instability. The improvement in passivation can be linked to an increase in SiH* emission intensity (inset of Figure 1b). The SiH$_4$ is highly depleted at low FR conditions due to higher RF power available per molecule; at the particular condition, the depletion factor reduces with an increase in FR.[11,25] However, in the case of 70 sccm, we have observed a maximum dissociation of SiH$_4$ (highest counts of SiH*) in plasma, but a relatively lower lifetime is observed. Further, with the 80 sccm FR condition, the deteriorated passivation can be due to some modifications in secondary reactions of chemical species produced in the plasma with the SiH$_4$ and H$_2$.[15] Highly diluted SiH$_4$ is generally used to deposit μc-Si thin films. As the dilution is not sufficient here, it is expected to obtain a-Si:H films close to the transition zone, with high interface passivation quality. However, as the plasma density could be low at very low FRs[26] and, hence, the passivation quality is not as expected at low FRs, and it improves with an increase in FR up to an intermediate value. Higher FR condition lowers the SiH$_4$ depletion due to insufficient RF power per molecule and low residence time of SiH$_4$ molecules. This may also cause the formation of a-Si:H films with a high density of DBs and weak Si–Si bonds. Therefore, the interface passivation quality drops at too high FRs.

In principle, the probability of SiH$_{x\leq 2}$ gas-phase scavenging reactions is reduced at low FRs of SiH$_4$, and therefore the SiH$_2$/SiH$_3$ contribution ratio should decrease with FR.[15,17] However, the SiH$_2$/SiH$_3$ ratio also depends on the electron temperature of the plasma, as a higher average electron temperature increases the formation of SiH$_2$ radicals. Depending on the interdependence of the plasma parameters, the electron temperature, as well as the plasma density, could reach a maximum value at an intermediate FR, and therefore the SiH$_2$/SiH$_3$ ratio reaches a maximum at the corresponding FR. Another factor is the transient plasma instability after ignition, which can affect the interface. It is visually observed that at low FRs, the temporary instability is prolonged; hence, it could affect the surface passivation quality, despite high SiH$_4$ depletion conditions. Therefore, it requires optima in SiH$_4$ depletion, electron temperature and plasma density, the flux of radicals toward the substrate, and transient plasma instability for a good level of surface passivation, which is obtained at intermediate FR.

Figure 4a shows the variation of optical bandgap (E_g) and refractive index at 1 eV (n_{1eV}) (estimated from ellipsometry data), and hydrogen content (estimated from Fourier transform infrared [FTIR] spectra) as a function of gas total FRs. The E_g and n_{1eV} are slightly sensitive to the gas FRs. The variation of E_g represents the hydrogen content difference in the film; an enhancement of E_g up to >1.7 eV with an intermediate FRs indicates the passivation of some of the tail/bulk defect states in the electronic bandgap with the better H-content. The similar trend of n_{1eV} as a function of gas FRs, with the relatively higher values, indicates film compactness or high film density with the Si–H
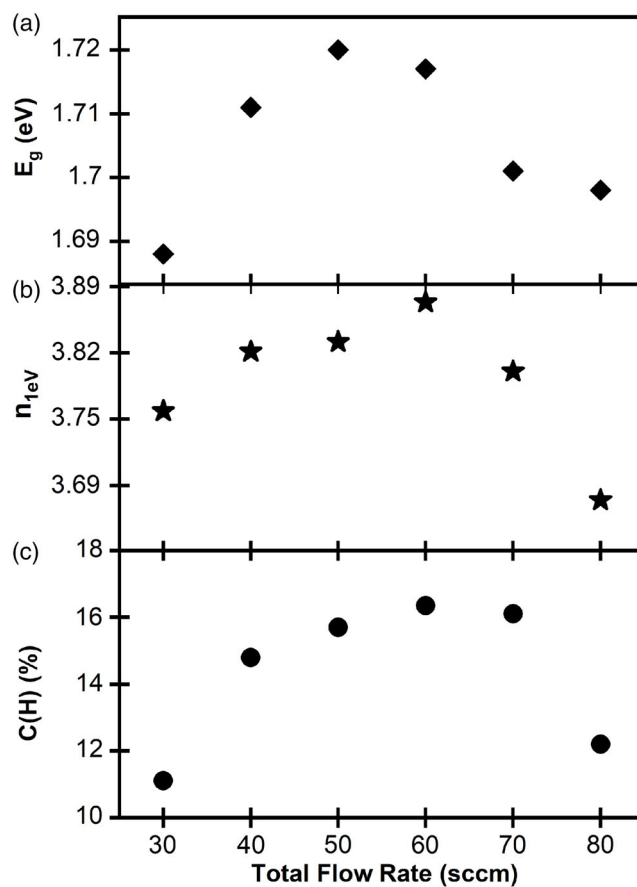
Figure 4. Variation of a) optical bandgap E_g, b) refractive index at 1 eV (n_{1eV}), and c) total hydrogen content C_H of the i-a-Si:H films with FR.

bonding environment. The (high) density shows better surface passivation with the Si–H content than the Si–H$_2$ content, which is slightly more porous and unable to provide better passivation. The C_H was estimated from the FTIR spectra related to the Si–H bonds of low- and high-stretching vibration modes at 2000 and 2100 cm^{-1} of the i-a-Si:H films with the assumption of negligible free hydrogen content in the film using the relation[27]

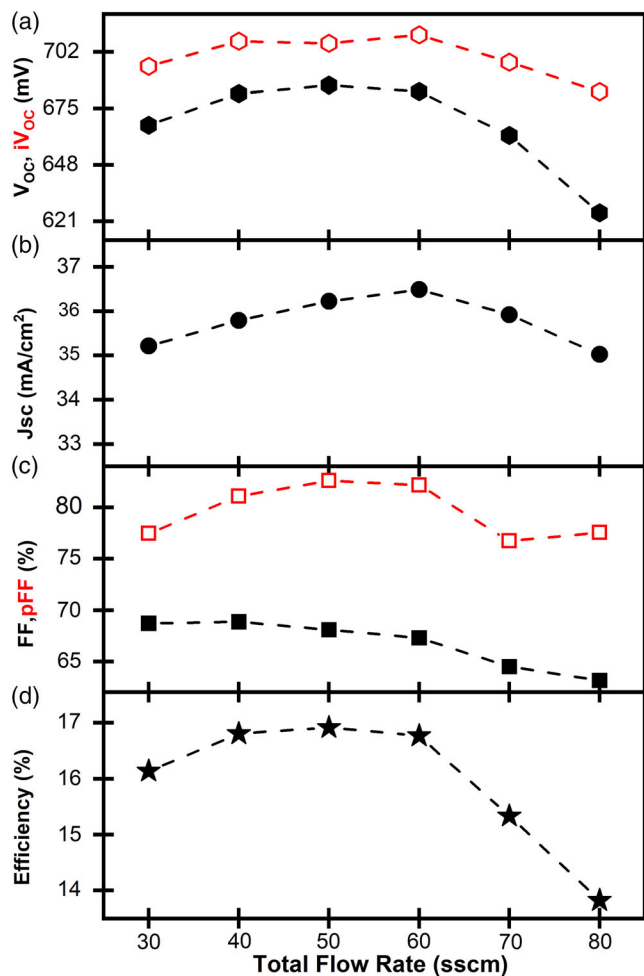$$C_H = \frac{A}{N} \int \frac{\alpha(\omega)}{\omega} d\omega \times 100 \ at.\% \tag{2}$$

where "A" denotes the proportionality constant of the Si–H$_n$ bonding modes, $A = 9.0 \times 10^{19}$ and 2.2×10^{20} cm^{-3} for the low- and high-stretching modes, respectively, "N" is the atomic density of Si (5×10^{22} cm^{-3}), and α is the absorption coefficient for high- and low-stretching modes and ω is the wavenumber.

One can see the C_H variation in the ≈200 nm i-a-Si:H film as a function of the FR (Figure 4c); relatively more C_H content with the intermediate FRs (40–70 sccm) is observed. This also supports the optical bandgap and film density variation. The C_H enhancement is due to the better decomposition of the SiH$_4$ molecules and an increase of precursor flux to the substrate surface after the dissociation. This also influences the microstructure factor; it signifies better c-Si surface passivation,[28] which is presented and discussed in the latter part of the text.

2.2. Gas FR Variation on SHJ Cell Performance

Figure 5 shows the SHJ cells' photovoltaic parameters, iV_{oc}, and pseudo fill factor variation (pFF) with the gas FRs for the i-a-Si:H layer deposition. The pFF is obtained from the Suns-V_{oc} measurement of the complete cell, which represents the FF of the cell without the contribution of series resistance. The passivation quality of the i-a-Si:H layers is also reflected in cell performance with a nearly similar trend. The difference between the iV_{oc} and V_{oc} is due to some process-induced damage during ITO (sputter) deposition and metallization (thermal evaporation).[28,29] A significant difference between the FF and pFF is due to the carrier transport resistive losses in the bulk of the i-a-S:H/p-a-Si:H stack, and at the hole- (p-a-Si:H/i-a-Si:H/n-c-Si) and electron-selective (n-c-Si/i-a-Si:H/p-a-Si:H) contacts, and also limited c-Si surface passivation. The FF can be enhanced further by optimizing the process parameters further with minimizing the cell's series resistance. Finally, we have fabricated the SHJ cell with the power conversion efficiency of $\approx 17\%$ with the gas FR of 60 sccm
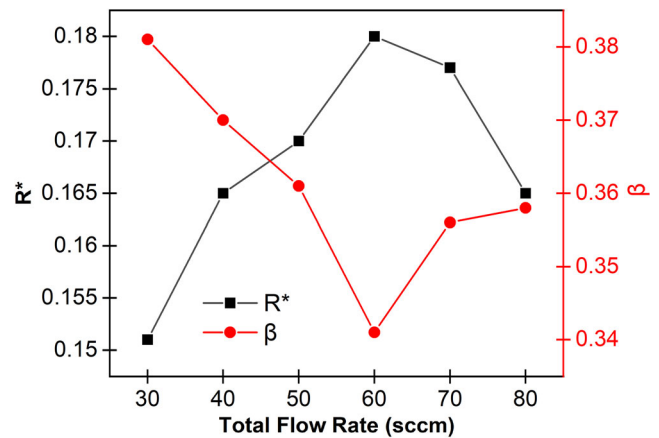
Figure 6. Microstructure factor (R*) and parasitic absorption losses (β) with different gas FRs.

for the i-a-Si:H layer deposition by keeping all other process parameters fixed.

Along with the passivation variation with gas FRs for the i-a-Si:H deposition, to identify the change in photocurrent density of a device after the i-a-Si:H incorporation, microstructure factor (R*)[28] and parasitic absorption losses (β)[30] are analyzed and presented in **Figure 6**. We have noticed a slight change in "β" with the i-a-Si:H layer deposition condition (since p-a-Si:H and ITO are identical for all devices). The minimum absorption loss has been observed from the 60 sccm gas FR condition, and "β" has an inverse relation with the R* of the i-a-Si:H layer with the gas FR. So, an increase in R* decreases the parasitic absorption loss, but beyond 60 sccm conditions, the R* values started to decline, and parasitic loss enhanced. The magnitude of current loss is also explained by considering the variation in the absorption coefficient and collection probability of photogenerated carriers within the stack apart from the absorption losses due to the i-a-Si:H layer thickness in SHJ solar cell. This analysis supports the cells' photocurrent variation with the gas FRs.

3. Conclusion

In this study, initially, we have investigated the c-Si surface passivation with the i-a-Si:H layers with the variation in the FR of SiH_4:H_2 gases, followed by the SHJ solar cells' photovoltaic parameters based on the gas FR. Optimized gas FR of 50–70 sccm are observed with the fixed gas pressure, substrate temperature, and applied power density for the relatively better c-Si surface passivating thin i-a-Si:H layers, which led to the τ_{eff} of >1 ms, iV_{oc} of ≈ 710 mV, and D_{it} of $\approx 3.5 \times 10^9$ cm^{-2} eV^{-1}. Finally, an SHJ cell with $\approx 17\%$ power conversion efficiency is fabricated with the optimized gas FR of 50–60 sccm for the i-a-Si:H layer deposition. With the gas FR variation, one can optimize the transient plasma instability, SiH_4 depletion, secondary reactions in the plasma, and flux of radicals toward the substrate for the better i-a-Si:H thin-film growth to minimize the c-Si DBs effectively for reducing minority carrier recombination.

Figure 5. a) Open-circuit voltage (V_{oc}) and implied V_{oc} (iV_{oc}), b) photocurrent density (J_{sc}), c) fill factor (FF) and pseudo fill factor (pFF), and d) power conversion efficiencies of the silicon heterojunction (SHJ) solar cells fabricated with buffer i-a-Si:H layers deposited from variable gas FRs. Lines are only the guide to the eyes.

4. Experimental Section

Intrinsic a-Si:H films were deposited on both sides of n-type Si wafers (Float-zone, $250 \pm 20\,\mu m$, $1–3\,\Omega\,cm$) by the PECVD deposition system (Excel Instruments) using the RF 13.56 MHz power generator. As-cut wafers were anisotropically etched using $\approx 2\,wt\%$ potassium silicate solution with isopropyl alcohol as an additive for 50 min at 80 °C, and an average pyramid height of 3–5 μm was obtained. The textured wafers were cleaned by the standard Radio Corporation of America (RCA) cleaning procedures, RCA1 and RCA2, to remove organic and inorganic contaminants, respectively. Before loading into the load lock chamber, the cleaned wafers were given 1% hydrofluoric acid dip for 1 min to remove native oxide, followed by drying in a nitrogen atmosphere. Silane and hydrogen gas mixture was used to grow i-a-Si:H layer with the PECVD reactor chamber volume of $\approx 15\,L$. The interelectrode distance was fixed at $\approx 20\,mm$, and substrates were mounted on the top electrode in the chamber. The fixed deposition parameters are 1) substrate temperature ≈ 230 °C; 2) the deposition pressure (P_r) of 1 Torr; 3) power density P_w of $44\,mW\,cm^{-2}$; and 4) SiH_4/H_2 dilution ratio = 1. Films were deposited at different total gas FRs ranging from 30 to 80 sccm in steps of 10 sccm. The $\approx 10\,nm$ i-a-Si:H films were symmetrically deposited on the c-Si substrate to evaluate the quality of textured c-Si surface passivation.

In situ OES fiber optic spectrometre from the Ocean Optics (HDX model) was used to analyze the presence of hydrogen- and silane-related species in the plasma, and the spectra were captured after obtaining stable plasma. [Correction added after publication 18 August 2022: A typo was corrected in the preceding sentence]. The optical emission peaks of interest were the Balmer H_α line (656.3 nm) and SiH* line (414 nm), which were captured in a sampling time of 15 ms. The effective minority carrier lifetime of symmetrically passivated test structures was measured using a Sinton WCT-120TS lifetime tester either in the transient or generalized mode. Single-sided polished wafers were used for ellipsometry and FTIR measurements. The $\approx 10\,nm$ passivating film was analyzed using Variable Angle Spectroscopic Ellipsometry (J.A. Woollam, M-2000, USA), and the Tauc–Lorentz (TL) model was used for estimating the films' electronic bandgap and density. The hydrogen content and microstructure factor of $\approx 200\,nm$ a-Si:H films were determined from the FTIR spectroscopy (Thermo-fisher Nicolet iS50) in the transmission mode.

For solar cells fabrication, a stack of $\approx 10\,nm$ i-a-Si:H/$\approx 10\,nm$ n-a-Si:H was first deposited on the rear side of the c-Si wafer. After a short vacuum break, the wafers were flipped and loaded back into the PECVD chamber for deposition of the $\approx 10\,nm$ i-a-Si:H/$\approx 10\,nm$ p-a-Si:H stack on the front. For the n-a-Si:H layer deposition, the gas flow ratio of $H_2:SiH_4:PH_3 = 50:7.5:2.5$ (in sccm) were used at 1 Torr pressure and substrate temperature of 200 °C, and for the p-a-Si:H layer deposition, the ratio was $H_2:SiH_4:B_2H_6 = 50:5:5$ (in sccm) at 1 Torr pressure and substrate temperature of 180 °C. Afterward, RF magnetron sputtering was used to deposit indium tin oxide (ITO) films on the front and rear sides of the SHJ cell with thicknesses ≈ 70 and $\approx 130\,nm$, respectively. ITO layers were deposited at the power density of $1.5\,watt\,cm^{-2}$, the substrate temperature of ≈ 120 °C, and deposition pressure was maintained at 4 mTorr. During the ITO film deposition, the substrate holder was rotated at the 30 RPM speed (to get a better uniformity of the film) at the fixed 10 cm distance from the magnetron. Silver was thermally evaporated using a shadow mask to form the front Ag grid, and Al was used as the back electrode. The area of the fabricated cell was $1.7 \times 1.7\,cm$ having a front metal shading of $\approx 7\%$. The J–V characteristics of the cells were recorded using a Class AAA solar simulator (Oriel Sol3A, Newport, USA) under standard 1 sun illumination conditions ($100\,mW\,cm^{-2}$, Air Mass 1.5, 25 °C). The system was calibrated with a standard reference cell certified by the National Renewable Energy Laboratory, USA. The external quantum efficiency and reflection measurement were conducted using a quantum efficiency measurement system from the Bentham, UK.

Conflict of Interest

The authors declare no conflict of interest.

Data Availability Statement

The data that support the findings of this study are available from the corresponding author upon reasonable request.

[1] D. Adachi, J. L. Hernández, K. Yamamoto, *Appl. Phys. Lett.* **2015**, *107*, 22.

[2] M. Taguchi, A. Yano, S. Tohoda, K. Matsuyama, Y. Nakamura, T. Nishiwaki, K. Fujita, E. Maruyama, *IEEE J. Photovoltaics* **2014**, *4*, 96.

[3] K. Yoshikawa, H. Kawasaki, W. Yoshida, T. Irie, K. Konishi, K. Nakano, T. Uto, D. Adachi, M. Kanematsu, H. Uzu, K. Yamamoto, *Nat. Energy* **2017**, *2*, 17032.

[4] Y. Liu, Y. Li, Y. Wu, G. Yang, L. Mazzarella, P. Procel-Moya, A. C. Tamboli, K. Weber, M. Boccard, O. Isabella, X. Yang, B. Sun, *Mater. Sci. Eng. R Rep.* **2020**, *142*, 100579.

[5] K. Gotoh, M. Wilde, S. Kato, S. Ogura, Y. Kurokawa, K. Fukutani, N. Usami, *AIP Adv.* **2019**, *9*, 075115.

[6] T. Ruan, M. Qu, J. Wang, Y. He, X. Xu, C. Yu, Y. Zhang, H. Yan, *J. Mater. Sci. Mater. Electron.* **2019**, *30*, 13330.

[7] J. Ge, Z. P. Ling, J. Wong, R. Stangl, A. G. Aberle, T. Mueller, *J. Appl. Phys.* **2013**, *113*, 234310.

[8] J. Mitchell, D. Macdonald, A. Cuevas, *Appl. Phys. Lett.* **2009**, *94*, 162102.

[9] A. Matsuda, M. Takai, T. Nishimoto, M. Kondo, *Sol. Energy Mater. Sol. Cells* **2003**, *78*, 3.

[10] A. Matsuda, *J. Vac. Sci. Technol., A* **1998**, *16*, 365.

[11] A. Descoeudres, L. Barraud, R. Bartlome, G. Choong, S. De Wolf, F. Zicarelli, C. Ballif, *Appl. Phys. Lett.* **2010**, *97*, 183505.

[12] U. K. Das, M. Z. Burrows, M. Lu, S. Bowden, R. W. Birkmire, *Appl. Phys. Lett.* **2008**, *92*, 063504.

[13] J.-C. Hsiao, C.-H. Chen, C.-C. Lin, D.-C. Wu, P. Yu, *J. Electrochem. Soc.* **2011**, *158*, H876.

[14] J. Panigrahi, V. K. Komarala, *J. Non-Cryst. Solids* **2021**, *574*, 121166.

[15] A. Matsuda, *Jpn. J. Appl. Phys.* **2004**, *43*, 7909.

[16] E. Özkol, P. Wagner, F. Ruske, B. Stannowski, L. Korte, *Phys. Status Solidi A* **2022**, *219*, 2100511.

[17] C. Niikura, N. Itagaki, A. Matsuda, *Jpn. J. Appl. Phys.* **2007**, *46*, 3052.

[18] A. A. Howling, B. Strahm, P. Colsters, L. Sansonnens, C. Hollenstein, *Plasma Sources Sci. Technol.* **2007**, *16*, 679.

[19] S. Olibet, E. Vallat-Sauvain, C. Ballif, *Phys. Rev. B: Condens. Matter Mater. Phys.* **2007**, *76*, 035326.

[20] C. Leendertz, N. Mingirulli, T. F. Schulze, J. P. Kleider, B. Rech, L. Korte, *Appl. Phys. Lett.* **2011**, *98*, 2009.

[21] R. B. M. Girisch, R. P. Mertens, R. F. De Keersmaecker, *IEEE Trans. Electron Devices* **1988**, *35*, 203.

[22] A. Richter, S. W. Glunz, F. Werner, J. Schmidt, A. Cuevas, *Phys. Rev. B* **2012**, *86*, 165202.

[23] R. A. Sinton, A. Cuevas, *Appl. Phys. Lett.* **1996**, *69*, 2510.

[24] S. De Wolf, H. Fujiwara, M. Kondo, in *2008 33rd IEEE Photovolatic Spec. Conf.*, Vol. *1*, IEEE, Piscataway, NJ **2008**, pp. 1–4.

[25] S. I. Ishihara, M. Kitagawa, T. Hirao, K. Wasa, T. Arita, K. Mori, *J. Appl. Phys.* **1987**, *62*, 485.

[26] B. B. Sahu, J. G. Han, K. S. Shin, K. Ishikawa, M. Hori, Y. Miyawaki, *Plasma Sources Sci. Technol.* **2015**, *24*, 025019.

[27] A. A. Langford, M. L. Fleet, B. P. Nelson, W. A. Lanford, N. Maley, *Phys. Rev. B* **1992**, *45*, 13367.

[28] H. Sai, P. W. Chen, H. J. Hsu, T. Matsui, S. Nunomura, K. Matsubara, *J. Appl. Phys.* **2018**, *124*, 103102.

[29] D. Zhang, A. Tavakoliyaraki, Y. Wu, R. A. C. M. M. van Swaaij, M. Zeman, *Energy Procedia* **2011**, *8*, 207.

[30] Z. C. Holman, A. Descoeudres, L. Barraud, F. Z. Fernandez, J. P. Seif, S. De Wolf, C. Ballif, *IEEE J. Photovoltaics* **2012**, *2*, 7.